

The Permian-Triassic low sulfidation epithermal Au deposit of Don Sixto, Mendoza

Ana Cecilia MUGAS LOBOS¹, María Florencia MÁRQUEZ-ZAVALÍA^{2,3}, Miguel Ángel GALLISKI², and Markus WÄLLE⁴

¹ Centro de Investigaciones de la Geósfera y la Biósfera (CIGEOBIO- CONICET), San Juan.

² Instituto Argentino de Nivología, Glaciología y Ciencias Ambientales (IANIGLA- CONICET). Mendoza.

³ Mineralogía y Petrología, Licenciatura en Cerámica Industrial, Universidad Nacional de Cuyo, Mendoza.

⁴ Institute of Geochemistry and Petrology, Department of Earth Sciences, ETH Zurich, Zurich, Switzerland.

Email: amugas@unsj-cuim.edu.ar

Editor: Mónica López de Luchi

ABSTRACT

Don Sixto is a 252.7 ± 1.3 Ma low sulfidation epithermal Au deposit located in Mendoza, Argentina. The mineralization in this area (~ 4 km²) reaches a gold resource of 1,258,000 ounces, occurring as Au-quartz veins and Au-dissemination in volcanic-pyroclastic units closely related to the Choiyoi magmatism. Seven stages of mineralization were recognized, where quartz is the major gangue mineral with lesser adularia and fluorite (\pm calcite). The most representative vein textures are massive, crustiform, and comb. Bladed quartz together with adularia (\pm calcite) were recognized in the stages 2 and 4. Abundant pyrite and lesser arsenopyrite, chalcopyrite and sphalerite were recognized in most stages. Gold has variable fineness and occurs mainly in the stage 4, together with scarce uytengbaardite, acanthite and Se- and Te-bearing minerals. Microthermometry data indicate that mineralizing fluids were diluted (< 5.16 wt% CINA_{equiv}) with average homogenization temperatures reaching < 316.0 °C. LA-ICP-MS results indicate that the highest values of Na, K and S were reached in the stage 4 and 5, closely related to boiling conditions in the former. In general, a limited data set was obtained due to the small size of the fluid inclusions and the low signals that prevented analysis, which are common characteristics of low sulfidation deposits. The stable isotope data $\delta^{18}\text{O}_{\text{H}_2\text{O}}$ indicate a major meteoric water source for the oxygen in the fluids. Regarding $\delta^{34}\text{S}$, the preliminary value does not define a unique source; instead a mixed one is feasible between magmatic source and a possible contribution from the sedimentary Agua Escondida Formation.

Keywords: *Mineralogy, quartz veins, fluid inclusions, LA-ICP-MS*

RESUMEN

Don Sixto, un depósito de Au de baja sulfuración del Pérmico-Triásico, Mendoza.

Don Sixto es un depósito epitermal de baja sulfuración de $252,7 \pm 1,3$ Ma, ubicado en Mendoza, Argentina. La mineralización en esta área (~ 4 km²) se desarrolla en vetas de cuarzo-Au y Au-diseminado en las unidades volcánico-piroclásticas asociadas al magmatismo Choiyoi, alcanzando un recurso aurífero de 1.258.000 onzas. Siete estadios de mineralización fueron identificados, siendo el cuarzo el mineral de ganga mayoritario y en menor medida, adularia y fluorita (\pm calcita). Las texturas de veta más representativas son maciza, crustiforme y en empalizada. La asociación de textura de reemplazo según calcita en cuchilla (bladed quartz) y cristales de adularia fue identificada en los estadios 2 y 4. Abundante pirita y en menor medida arsenopirita, calcopirita y esfalerita están presentes en la mayoría de los estadios. El oro se encuentra principalmente en el estadio 4, asociado a escasa uytengbaardita, acantita y minerales de Se y Te. Los resultados microtermométricos indican que los fluidos mineralizantes estaban diluidos ($< 5,16$ wt. % CINA_{equiv}) y tenían temperaturas de homogeneización promedio de $< 316,0$ °C. Los valores más altos de Na, K y S están asociados a los estadios 4 y 5, en el primer caso estrechamente relacionado a condiciones de ebullición. Los resultados de LA-ICP-MS fueron escasos debido a que el pequeño tamaño de las inclusiones y la baja señal analítica impidieron el análisis. Los resultados de $\delta^{18}\text{O}_{\text{H}_2\text{O}}$ indican una fuente meteórica para el oxígeno en los fluidos mineralizantes; los resultados preliminares de $\delta^{34}\text{S}$ no pueden definir una única fuente para el azufre; siendo posible un origen mixto.

Palabras clave: *Mineralogía, vetas de cuarzo, inclusiones fluidas, LA-ICP-MS.*

INTRODUCTION

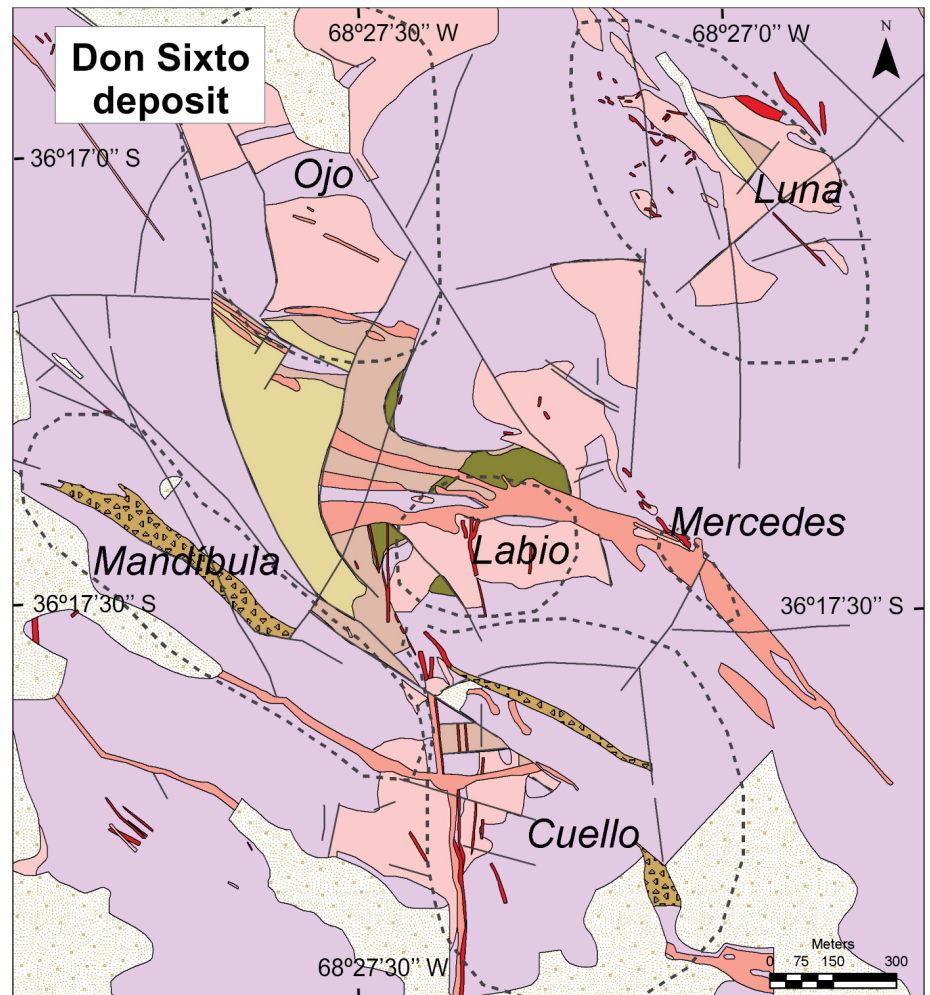
Don Sixto is an epithermal low sulfidation precious metal deposit hosted by volcanic and pyroclastic sequences of Permian-Triassic age. This deposit is located at the southeast of Mendoza province, in the San Rafael Massif, Argentina (Fig. 1). The alteration halo of Don Sixto deposit was first pointed out in 1996 while doing a Landsat imagery exploration. Subsequent exploration programs on the basis of geologic mapping and geochemistry led to the delimitation of the gold mineralization; the main prospects in Don Sixto deposit are: Cuello, Labio, Ojo, Luna, Mercedes and Mandíbula (Fig. 1). More than 20,000 m of rock were drilled by the owner mining company and the gold resources were calculated at 1,258,000 ounces with a cut-off grade of 0.5 g/t Au (Van der Heyden and Yeo 2007), including measured and indicated resources (924,000 ounces at 1.4 g/t Au) and inferred resources (334,000 ounces at 1.12 g/t Au). The average gold and silver grades in the deposit are 1.45 g/t and 5.21 g/t respectively.

Carpio *et al.* (2001), Rubinstein *et al.* (2001), Godeas and Rubinstein (2004), Rubinstein and Gargiulo (2005), Delendatti (2005) and Narciso *et al.* (2007) worked on specific aspects of this deposit. Recently, Mugas Lobos *et al.* (2010, 2011, 2012a, b), Mugas Lobos (2012) and Mugas Lobos and Márquez-Zavalía (2013) gave more comprehensive descriptions of Don Sixto deposit.

The aim of this contribution is to give a thorough description of the deposit. In order to accomplish this goal a complete characterization of the epithermal vein system was done; the vein mineralogy was described as much as the fluid inclusion studies and stable isotope data. New reflectance spectroscopy results obtained from hydrothermally altered samples, as well as the age of the deposit and new LA-ICP-MS results, along with the other data, are presented, discussing them in relation with previous data produced in the area.

REGIONAL AND LOCAL GEOLOGY

During the late Carboniferous-early Permian to Triassic, a widespread magmatism took place in northern and central Chile and Argentina. This plutonic-volcanic association has been known as the Choiyoi province (Kay *et al.* 1989). The Permian-Early Triassic was the period of highest development for this magmatism (Llambías 1999); the mesosilicic and silicic igneous complexes north of 39° S cover an area of at least 200,000 km² in central



References

- Prospects
- Faults
- Recent alluvial deposits
- Basalts
- Don Sixto breccia
- Quartz veins
- El Portillo Group (rhyolite)
- Choique Mahuida Formation (rhyolite)
- Choique Mahuida Formation (ignimbrite)
- Choique Mahuida Formation (pyroclastic lenticular deposits)
- Agua Escondida Formation (sandstone)
- Agua Escondida Formation (shale)

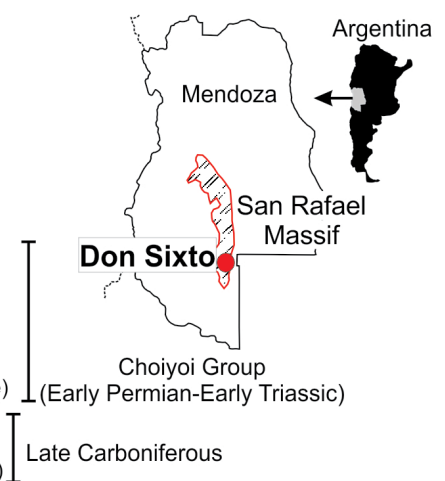


Figure 1. Geologic sketch of the Don Sixto deposit (modified from Delendatti and Williams 2007, Van der Hayden and Yeo 2007).

ian to Triassic, a widespread magmatism took place in northern and central Chile and Argentina. This plutonic-volcanic association has been known as the Choiyoi province (Kay *et al.* 1989). The

Permian-Early Triassic was the period of highest development for this magmatism (Llambías 1999); the mesosilicic and silicic igneous complexes north of 39° S cover an area of at least 200,000 km² in central

western Argentina and central Chile, and even more than 500,000 km² according to information from oil exploration boreholes (Llambías *et al.* 2003). In Argentina, the volcanic-pyroclastic sequences of this magmatism are associated in the Choiyoi Group (Stipanovic *et al.* 1968), where two different sections were identified: a lower section represented by andesites, dacites and rhyolites, and an upper section, mainly rhyolitic (Llambías *et al.* 1993). The genesis of these rocks was interpreted as typical of a transitional geotectonic environment, in between a volcanic arc and an intraplate post-orogenic distensive magmatic-tectonic environment, represented in the lower and upper section of the Choiyoi Group respectively (*e.g.*, Llambías *et al.* 1993, Kleiman 1993, Ramos 1999, Llambías 1999, Kleiman and Japas 2009). In Don Sixto deposit (Figs. 1, 2a), the oldest rocks belong to the Late Carboniferous Agua Escondida Formation (González Díaz and García 1966), mainly composed of yellowish-brown fine to medium-grained sandstone, grey-greenish greywacke and black to dark grey-bluish shale, alternating with lenticular conglomerate deposits. These marine clastic rocks are unconformably overlain by the volcanic and pyroclastic sequences of the Choique Mahuida Formation (Linares *et al.* 1978), with a regional early Permian-Late Triassic age (Narciso *et al.* 2007), and partially equivalent to the Cerro Carrizalito Formation (González Díaz 1972), with a zircon U/Pb (SHRIMP) age of 252.3 ± 3.8 Ma and 251.9 ± 2.7 Ma (Rocha-Campos *et al.* 2006, 2011, respectively). The Choique Mahuida Formation, included in the upper section of the Choiyoi Group (Stipanovic *et al.* 1968), is composed of rhyolite, rhyolitic ignimbrite (Fig. 2b) and isolated pyroclastic lenticular deposits. Rhyolites are widely distributed, especially in Cuello and Labio prospects; they are commonly light brown-yellowish to pink colored. Ignimbrites are welded to not welded and generally light brown-pinkish to dark grey colored. The pyroclastic lenticular deposits are scarce, commonly light brown-yellowish to medium grey colored and commonly occur in ≤ 0.60 to < 5 m thick lenses in association with ignimbrite in the subsurface of Cuello, Labio and Ojo prospects.

The subvertical dikes of the El Portillo

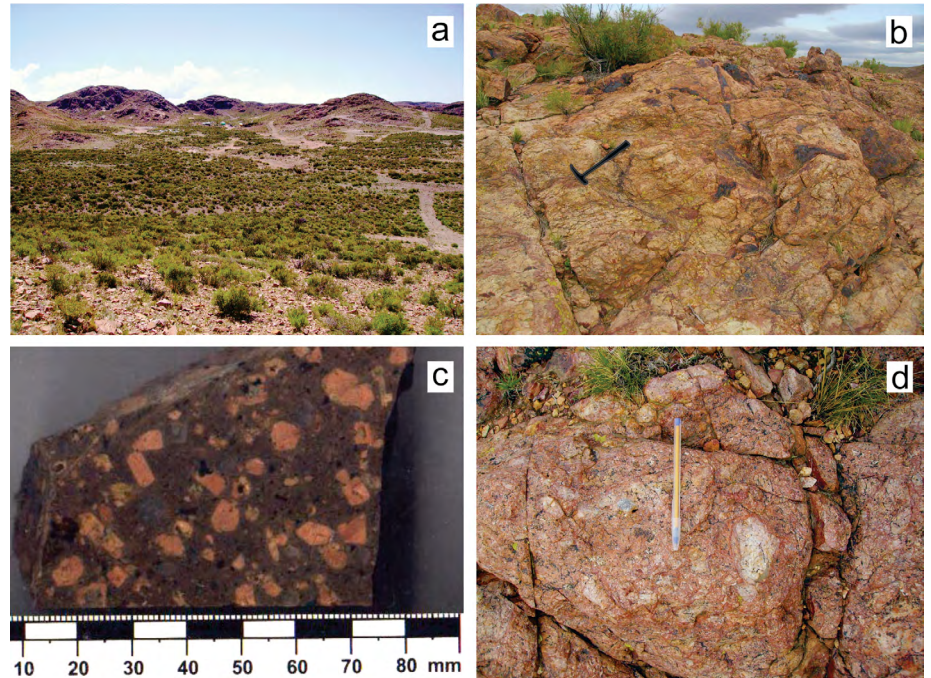


Figure 2. Photographs at outcrop scale (a, b, d) and hand specimen (c) showing: a) A general view of Don Sixto deposit; b) Rhyolite outcrop in Ojo prospect; the rocks are silicified and show moderate development of argillic alteration. The surface is partially tarnished by oxidized material; c) Rhyolite sample of El Portillo Group; d) Don Sixto breccia in Mandibula prospect.

Group (late Permian-Early Triassic) cross-cut the previous sequence, mainly with a NW-SE and N-S strike; these rocks are generally yellowish orange, coarse grained porphyry rhyolite (Fig. 2c). The average age of this Group, in the San Rafael Massif, is in the range between 250 and 240 Ma (Narciso *et al.* 2007).

Two hydrothermal breccia bodies, Don Sixto and the Silicea breccias, were identified in the area. The former is red in color, composed by irregular fragments of quartz veins and altered volcanic rocks with accessory oxidized sulfides, cemented by microcrystalline limonite-tarnished quartz (Figs. 2d, 3a). The grey colored Silicea breccia is composed of irregular fragments of light-grey quartz veins and subordinated fragments of strongly silicified volcanic rocks, set in a sericitized matrix with scarce sulfides, all cemented by microcrystalline quartz (Fig. 3b). The development of these two breccia bodies was controlled by major regional fault zones of NW-SE strike.

Hydrothermal alteration

The hydrothermal alteration is mostly pervasive, characterized by a strong to moderate silicification, moderate to strong

sericitization and weak to moderate development of argillic and propylitic alterations. The silicification is widely distributed in all the deposit and in different grades, quartz replaces all rock types. Sericitic and argillic alterations affect mainly the feldspar and glassy components in the volcanic and pyroclastic rocks; the presence of quartz-sericite/muscovite-pyrite >> chlorite-group minerals is characteristic. The most common products of argillic alteration are montmorillonite and kaolinite, whereas the presence of chlorite group minerals-pyrite-quartz-calcite-epidote >> adularia/albite, montmorillonite, illite, muscovite, magnetite-hematite characterizes the propylitic alteration.

Reflectance spectroscopy was performed in strongly altered samples, where major amounts of illite and smectite with lesser kaolinite and chlorite-group minerals were recognized together with goethite and hematite. The occurrence of illite, highly crystalline illite and kaolinite (Figs. 4a, b) in Cuello and Labio prospects is related to average Au grades of 1.83 and 2.51 g/t, respectively, whereas smectite (Fig. 4c) in Luna prospect is related to average Au grades of 1.58 g/t.

The presence of buddingtonite (Fig. 4d),

previously reported by Godeas and Rubinstein (2004), was confirmed in close relationship to illite and high average Au grades (1.63 g/t, Ojo prospect).

MATERIALS AND METHODS

Reflectance spectroscopy of hydrothermally altered samples was performed with a portable ASD-FieldSpec Pro RS3™, with a range detection capacity in between 350 and 2500 nm (nanometers), a resolution of 10 nm and a sampling interval of 1 nm. The spectrums were obtained with a high-intensity ASD probe with a visual-field of 1cm diameter; each spectrum is an average of 50 measurements (0.1 seconds for each, with a total measurement time of 5 seconds), obtained in relation to the Spectralon® white-standard. All spectrums were corrected with the ASD ViewSpec™ Pro software; false absorptions were minimized with the Splice Correction tool. The interpretation of spectrums was done with the SpecMin™ reference mineral spectral library and mineral spectral identification system for SWIR spectroscopy and the SpecWin1, plot and display program for spectral data.

Most of the microthermometric data were obtained with a Fluid Inc. adapted USGS gas-flow heating/freezing stage, mounted on a Leitz Laborlux transmitted light polarizing microscope at the Alfred Stelzner Museum, Universidad Nacional de Córdoba, Argentina. The instrumental precision is $\pm 0.1^\circ\text{C}$ between -56.6°C and 660.4°C ; apparent salinity of the natural fluid inclusions were indirectly obtained following Bodnar (1993) and Bodnar and Vityk (1994) and were reported in wt% $\text{NaCl}_{\text{equiv}}$. Calibration was performed on synthetic fluid inclusion standards by SYN FLINC to $\pm 0.2^\circ\text{C}$ at the melting points of CO_2 (-56.6°C) and H_2O (0.0°C), and to $\pm 3^\circ\text{C}$ at the critical point of pure H_2O (374.1°C). Additional data were measured on a Linkam THSMG-600 heating/freezing stage mounted on a Leitz Wetzlar POL microscope combined with a Hamamatsu C5810 3CCD camera and a Nikon Eclipse E600 POL microscope combined with a Nikon digital DXM 1200F camera, at the Department of Earth Sciences, ETH, Zürich, Switzerland, using

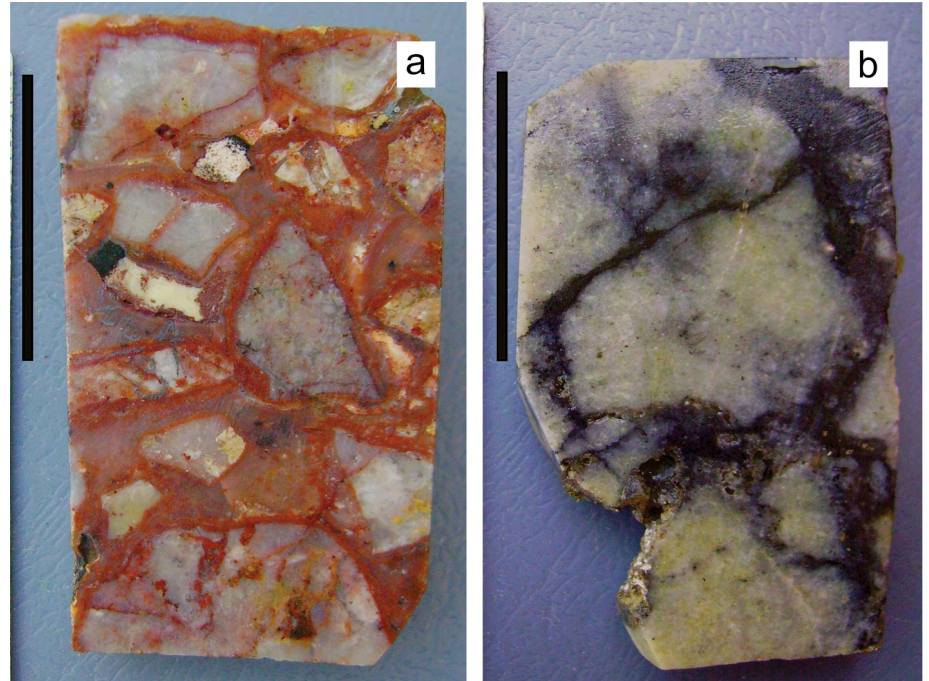


Figure 3. Hand samples of: a) Don Sixto breccia; b) Silicea breccia; bar scale= 2cm.

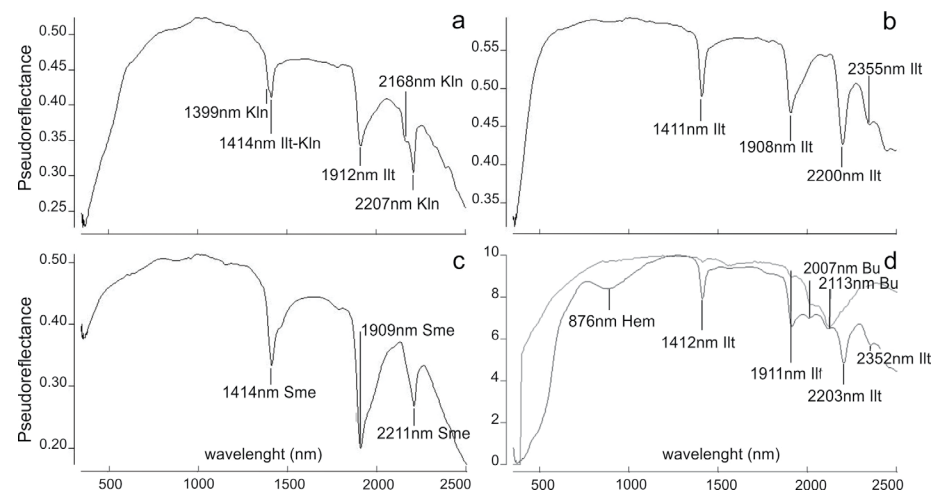


Figure 4. Mineral spectra of: a) Kaolinite-illite (Kln-Ilt); b) illite (Ilt); c) smectite (Sme); d) illite-hematite-buddingtonite (Ilt-Hem-Bu). Diagnostic absorptions are indicated.

similar standards for calibration. Only drill core samples were selected for fluid inclusion studies to avoid re-equilibration due to surface exposure (Bodnar 2003). Fluid inclusion petrography was done following Goldstein and Reynolds (1994) criteria, on previously defined fluid inclusion associations (FIAs).

Laser ablation-inductively coupled plasma-mass spectrometry (LA-ICP-MS) studies were performed at the Department of Earth Sciences, ETH Zürich, Switzerland. A Perkin Elmer Elan 6100 ICP-MS instrument combined with ETH's prototype Lambda

Physik 193-nm ArF excimer laser system (Günther *et al.* 1998, Heinrich *et al.* 2003, Pettke *et al.* 2004) with an energy density of up to 25 J/cm^2 and a pulse frequency of 10 Hz was used for determining the composition of individual fluid inclusions from each assemblage. Aerosol transport with a He-Ar carrier gas from the sample to the ICP was ensured by using a $\sim 1 \text{ cm}^3$ internal volume ablation cell. A limited element menu was programmed, including Si, Na, S, K, Fe, Cu, As, Ag, Sb, Cs, Au and Pb in order to maximize the detection limit due to the small size (average $5\mu\text{m}$) of the fluid

inclusions. The dwell time for Au was 70 milliseconds (ms), 20 ms for Si, As, Ag and Sb, and 10 ms for the remaining elements. Absolute quantification of single inclusion LA-ICP-MS signals was carried out by integration of signal intensities for all elements, correction for machine drift and host mineral contributions, comparison of intensity ratios with the external NIST glass standard SRM-610, and referencing the ratios to the absolute concentration of Na of each fluid inclusion, previously estimated by microthermometry. Limits of detection were calculated for each analysis individually, using three times the standard deviation of the background measurement ($3\sigma_{BG}$) divided by element sensitivity (Longerich *et al.* 1996). SILLS software (Guillong *et al.* 2008) was used to reduce the data and calculate element concentrations, using an empirical correction for K as the second-most important salt component (Günther *et al.* 1998, Heinrich *et al.* 2003).

Oxygen and sulfur isotope analysis were performed in the Stable Isotope Research Facility (Indiana University, USA). The oxygen fractionation $^{18}\text{O}/^{16}\text{O}$ was obtained by the Clayton and Mayeda (1963) method, with BrF₅; using as standards: Kan Pyx 9-14-11 I, Kan Pyx 9-14-11 J, EMR-Qtz 9-1-11 K, NCS-Qtz 8-27-11 M, NCS-Qtz 8-27-11 N, and NCS-Qtz 9-1-11 M. The sulfur fractionation $^{34}\text{S}/^{32}\text{S}$ was obtained with a Costech 4010 EA element analyzer; using as standards: EMR-CP, ERE-Ag₂S, PQB₂, EMR-CP, ERE-Ag₂S, PQB₂, EMR-CP, ERE-Ag₂S, EMR-CP, PQB₂, ERE-Ag₂S. Corrected delta values are relative to VSMOW and VCDT, for oxygen and sulfur respectively. The isotopic fractionation factors for quartz-H₂O and pyrite-H₂S were calculated in the AlphaDelta website (Beaudoin and Therrien 1999-2016), where Zheng (1993) and Ohmoto and Rye (1979) equations were used for oxygen and sulfur respectively, together with the Th of the corresponding stage of mineralization. The $\delta^{18}\text{O}_{\text{H}_2\text{O}}$ and $\delta^{34}\text{S}_{\text{H}_2\text{S}}$ calculation was done right after.

The $^{40}\text{Ar}/^{39}\text{Ar}$ multiple step heat method was performed in a fresh adularia sample, in the Arizona Noble Gas Laboratory (ANGL), Arizona Geochronology Center (AGC), Tucson, AZ, USA. Adularia chips for $^{40}\text{Ar}/^{39}\text{Ar}$ analysis were irradiated at

the USGS TRIGA Reactor (Denver, Colorado) along with GA1550 biotite (98.79 ± 0.54 Ma (Renne *et al.* 1998) flux monitors to calculate J-factors and K₂SO₄ and CaF₂ salts to calculate correction factors for interfering neutron reactions. Following a 2 to 3 weeks cooling period to allow for the decay of short-lived isotopes, samples were loaded into the arms of a glass storage tree above a double-vacu-

um, resistance-heated furnace and heated to 120°C at the same time that the entire extraction line was baked for 48 hours at 220°C. Getters and furnace were independently degassed near the end of the bake-out. Samples were then dropped into the furnace and argon was extracted from each sample using a computer controlled step-heating routine. The temperature of the furnace is estimated to be

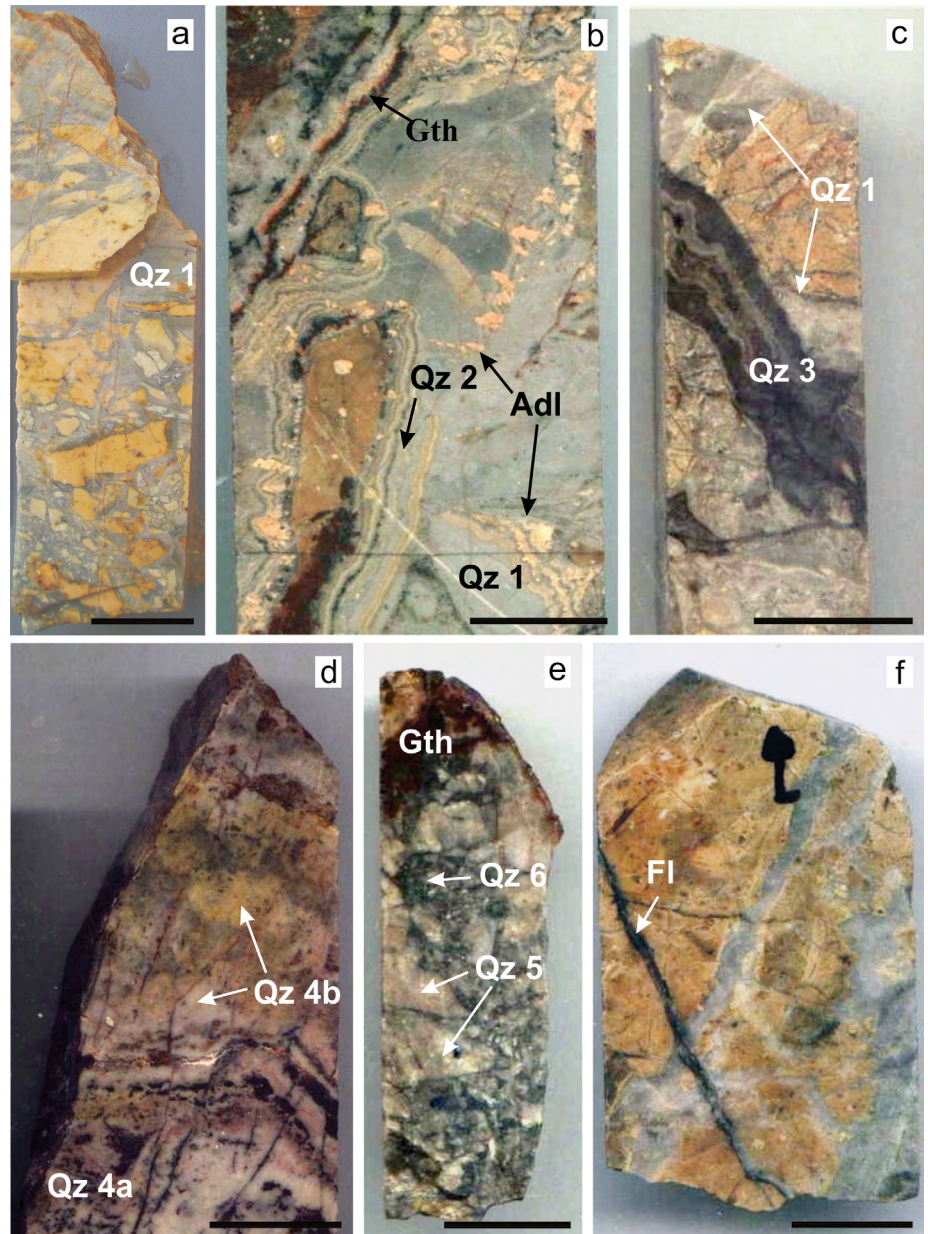


Figure 5. Mineralizing stages in Don Sixto deposit: a) Rhyolite fragments cemented by grey whitish massive quartz (Qz) from the stage 1; b) Rhyolite and massive quartz (stage 1) fragments cemented by crustiform-cockade textured quartz + adularia (Adl) + goethite (Gth) and scarce sulfides (stage 2); c) Rhyolite fragments cemented by massive quartz from stage 1, all crossed by a grey crustiform textured veinlet (stage 3); d) Quartz vein from the stage 4; bladed (Qz 4a) and massive (Qz 4b) textures occur together, the first one associated with limonites; e) Breccia sample with whitish massive quartz fragments from the stage 5 cemented by dark grey quartz from the stage 6; f) Rhyolite sample with several quartz veinlets of the stage 1, all crosscut by a fluorite (Fl) veinlet from the stage 7. Bar scale= 2.5 cm.

accurate to $\pm 20^\circ\text{C}$. Each heating step lasted 12 minutes, followed by a cool down to 500°C , prior to advancing the gas into two successive gettering stages for argon purification. The argon was then admitted into a VG 5400 mass spectrometer, where it was ionized and detected by a VG electron multiplier and digitized with a Keithley 617 Electrometer. Data collection and processing were accomplished using the computer program Mass Spec (Deino 2001). The decay constants used were those recommended by Steiger and Jäger (1977). Baseline values were subtracted and the isotopic measurements then were regressed to time zero using standard linear regression techniques. Additional corrections and associated uncertainties were applied to account for blanks, machine discrimination, atmospheric contribution, and interfering isotopes produced in the reactor from Ca, K and Cl present in the samples.

MINERALOGY

Mineralizing stages

Seven stages of mineralization were recognized in Don Sixto deposit on the basis of their mineralogy, vein texture and crosscutting relationships, each of them separated by successive vein opening and brecciation episodes (Figs. 5, 6). In this epithermal vein system quartz is the most abundant gangue mineral; lesser adularia (stages 2 and 4) and fluorite \pm calcite (stage 7) are also present. Primary infilling textures are common, banded, crustiform, comb and massive textures are well represented, while bladed replacement textures are locally present. Base metal minerals are widespread and occur in variable quantities in the different stages of mineralization (Fig. 6), usually with comparatively major amounts of pyrite; precious metal minerals, including sulfide, selenide and telluride minerals occur mainly in the stage 4, where repetitive boiling is believed to account for gold precipitation, with simultaneous separation of tellurium into the vapor phase and later deposition of Au-(Ag)-tellurides. Hematite and goethite are common supergenic minerals with lesser chalcocite, digenite and covellite that partially replace chalcopyrite.

Isolated quantities of anglesite were identified replacing galena. For further details about the mineralogy and mineral chemistry the reader is referred to Mugas Lobos (2012), Mugas Lobos *et al.* (2011, 2012a). *Stage 1:* This stage is well represented in most of the Don Sixto deposit. It is characterized by light-medium grey to white colored quartz, usually in <20 cm thick veins with usually massive texture and locally, banded and colloform textures. These quartz veins are common as stockwork and cementing rhyolite and/or ignimbrite fragments in the hydrothermal breccias (Fig. 5a). Ore minerals are very scarce, pyrite is dominant with lesser amounts of arsenopyrite, chalcopyrite, sphalerite, pyrrhotite and gold that may be locally present.

Stage 2: The veins from the second stage of mineralization are mainly distributed in Labio, Mercedes, Cuello and Luna prospects. They are usually thin veinlets (≤ 2 cm thick) characterized by the quartz-adularia mineral association (Fig. 5b); quartz is commonly white in color and chalcedony may be locally present. Adularia crystals are euhedral to sub-euhedral and sub-tabular habit is common. Massive texture is frequent together with banded, crustiform, colloform, cockade and lesser bladed replacement texture. Ore minerals are represented by pyrite, and lesser quantities of chalcopyrite, pyrrhotite and gold.

Stage 3: This stage is well represented in Cuello, Luna and Labio prospects. It is characterized by medium-dark grey quartz veins with banded and comb textures and lesser crustiform and colloform textures (Fig. 5c). Pyrite, arsenopyrite, chalcopyrite and sphalerite are the most common ore minerals, present in variable quantities in some cases associated with lesser amounts of bornite, pyrrhotite, marcasite, galena and hematite; gold, silver, stromeyerite and Se-enriched polybasite are not widespread but locally present. In Ojo and Mandíbula prospects this stage is represented by massive, light grey to white chalcedonic quartz veins with vugs and cavities usually filled with goethite.

Stage 4: This stage is well represented in Cuello, Luna and Labio prospects. In the Silicea breccia, fragments of quartz veins from previous stages are cemented by dark grey quartz with massive porous texture

from this stage. Here sericite, partially limonitized pyrite, gold and lesser amounts of base metal sulfides are frequent.

In general, this stage is characterized by light-medium grey colored quartz veins with bladed (Qz 4a; Fig. 5d), massive (Qz 4b) and banded textures; parallel, lattice and ghost bladed textures were identified (Qz 4a). Occasionally, bladed quartz occurs together with bladed calcite and/or microscopic adularia crystals which are indicative of a boiling process; observations that concord with the petrography of fluid inclusions. The main precious metal mineralization is related to this stage: gold (may be visible in hand specimens), silver, acanthite (occasionally enriched in selenium) and uytenbogaardtite, together with variable quantities of pyrite, arsenopyrite, chalcopyrite, sphalerite, lesser pyrrhotite, marcasite, bornite, galena, boulangerite, hematite, stützite and cervelleite (Fig. 6).

Stage 5: These quartz veins are commonly found as stockwork and breccias, cementing fragments of the previous quartz veins and fragments of rhyolite and ignimbrite in Cuello, Luna and Mandíbula prospects. It is represented by light-grey to white massive quartz veins (Fig. 5e), with minor banded and comb textures; variable amounts of chlorite-group minerals with pyrite, lesser chalcopyrite, sphalerite and pyrrhotite, associated with minor gold are common.

Stage 6: This stage is easily recognized for their dark-grey massive quartz, associated with abundant and partially limonitized pyrite, lesser amounts of arsenopyrite and variable quantities of chalcopyrite, sphalerite, pyrrhotite, marcasite, galena, magnetite, hematite, gold and silver (Fig. 6). This quartz is usually found cementing vein fragments of the stages 3 and 5 (Fig. 5e) or as stockwork in Cuello, Labio and Luna prospects.

Stage 7: Represented by thin veinlets and crusts of massive, purple-violet fluorite usually associated with variable quantities of quartz, calcite, pyrite and scarce arsenopyrite, chalcopyrite and/or sphalerite. Fluorite veinlets are well represented in Cuello prospect and may crosscut quartz veins from the stages 4, 5 and 6 (Fig. 5f).

Gangue minerals

In Don Sixto deposit the most abundant

and widespread gangue mineral is quartz, whereas fluorite, adularia and calcite are scarce.

Quartz is the most representative and abundant gangue mineral in Don Sixto deposit (Figs. 5, 6); light grey to milky white in color is common and more widespread compared to dark grey and transparent crystals. Primary, infilling textures are characteristic of this vein system; massive and crustiform with lesser banded textures are present in almost all mineralizing stages. Bladed replacement textures are well developed (parallel, lattice and ghost bladed) and are typically present in the stages 2 and 4, occasionally associated to bladed calcite and/or rhombic adularia, which indicate extensive boiling (Dong and Morrison 1995). Vein samples from the different stages were analyzed and most of them were suitable for fluid inclusion studies on the bases of mineral transparency and presence of FIAs.

Adularia is present in the stage 2 (Figs. 5b, 6) and in lesser quantities in the stage 4. The former is abundant and visible in hand specimens reaching up to 3 mm in size; it is pinkish-orange in color and has generally rhombic to subrhombic sections and sub-tabular habit. These crystals are commonly found developing crustiform, cockade and bladed textures in close association with quartz. Occasionally, pseudo-acicular crystals of adularia (pseudomorphs after calcite) were identified in bladed textures. Adularia crystals from the stage 4 are less abundant, they are microscopic in size (<60 μm) and typically rhombic. These crystals are commonly found associated to bladed quartz textures. Adularia crystals were not transparent enough for fluid inclusion studies. Fluorite is scarce and restricted to the stage 7 (Figs. 5f, 6). It commonly occurs as thin, massive, purple-violet veinlets, typically related to quartz, scarce pyrite and calcite, associated with sericite. Samples of fluorite were suitable for fluid inclusion studies with well sized and abundant FIAs.

Calcite is very scarce and occurs as platy and needle-shaped crystals in the center of lattice bladed quartz. This mineral was recognized in the stage 4, related to adularia and in the stage 7, associated with fluorite. Fluid inclusion studies were not

Stages	Hypogenic							Supergenic
	1	2	3	4	5	6	7	
Quartz	—	—	—	—	—	—	—	—
Adularia		—		—				
Fluorite							—	
Calcite				—				
Pyrite	—	—	—	—	—	—	—	
Arsenopyrite	—		—	—		—	—	
Chalcopyrite	—		—	—	—	—	—	
Sphalerite	—		—	—	—	—	—	
Pyrrhotite	—		—	—	—	—	—	
Marcasite						—		
Bornite			—	—				
Galena			—	—				
Boulangerite				—				
Magnetite				—				
Hematite				—				
Gold	—	—	—	—	—	—	—	
Silver			—	—		—	—	
Acanthite				—				
Stromeyerite			—	—				
Uytenbogaardtite				—				
Naumannite				—				
Polybasite			—	—				
Stützite				—				
Cervelleite				—				
Chalcocite							—	
Digenite							—	
Covellite							—	
Anglesite							—	
Hematite							—	
Goethite							—	

Figure 6. Simplified paragenetic sequence of the Don Sixto deposit. Full line: abundant; segmented line: scarce.

possible on calcite samples due to the small size of crystals.

Ore minerals

The base and precious metal mineral association includes comparatively major amounts of pyrite, though the total proportion of ore minerals in the veins is approximately 2% in volume.

Base metal minerals: Pyrite is abundantly widespread in all the stages of the mineralization. It occurs as euhedral to subhedral (10 to 600 μm), commonly zoned, isolated crystals and irregular aggregates (<1.5 mm) in quartz, frequently fractured in different grades, showing cracked textures, sometimes developing late porous crowns around the crystals. Pyrite, in different degrees, is commonly replaced by goethite.

Arsenopyrite is less abundant than pyrite and occurs in quartz as euhedral to subhedral rhombic grains (15 to 200 μm), irregular aggregates (150 a 900 μm) and rarely twinned on {012} to produce star-shaped trillings or cruciform twins. It is typically related to pyrite developing intergrowths; locally arsenopyrite occurs as crustifications over pyrite fringes or partially replacing that mineral. Occasionally, scarce inclusions of bornite (5 to 10 μm) and electrum (<12 μm) were recognized. Arsenopyrite is partially limonitized and partly replaced by covellite.

Chalcopyrite occurs as isolated anhedral grains (up to 250 μm) in quartz, as inclusions in pyrite and mainly associated to sphalerite developing chalcopyrite disease (Barton and Bethke 1987) textures. Chalcopyrite is locally replaced by poly-

basite and bornite, and partially to totally replaced by chalcocite, digenite and covellite.

Sphalerite occurs in quartz as isolated anhedral grains (30 to ~1000 μm) or developing irregular aggregates (<2 mm) with chalcopyrite. Besides the later, sphalerite grains are commonly found in association with pyrite, arsenopyrite and galena.

Pyrrhotite is scarce and occurs as isolated anhedral to subhedral grains (10 to 400 μm) and small inclusions in pyrite. Pyrrhotite grains are partially replaced by marcasite \pm pyrite \pm limonite, developing scale textures.

Marcasite is present as isolated, subtabular grains (20 to 270 μm), with frequent lamellar twinning, in quartz. It develops a scale texture (possible after pyrrhotite and/or pyrite) and fingerprint texture with concentric alternating thin bands of this mineral (after pyrrhotite) and goethite.

Bornite is scarce and occurs in patches, partially replacing chalcopyrite and partly replaced by digenite and covellite.

Galena occurs in quartz as isolated anhedral grains up to 100 μm , closely related to sphalerite, pyrite and arsenopyrite. Galena is partially replaced by covellite and in a lesser degree by anglesite. The content in Ag varies from 0.00 to 0.52 wt%.

Boulangerite is very scarce and was found as irregular to rounded inclusions in galena. Magnetite occurs as small (<50 μm) irregular grains, either isolated or in irregular aggregates (<400 μm) closely related to pyrite; hematite partially replaces magnetite.

Hematite is scarce and occurs as isolated tabular grains (10 to 130 μm) arranged in semiradial aggregates (<350 μm) in quartz; small inclusions in pyrite were also recognized.

Precious metal minerals: The precious metal-bearing minerals are generally scarce. They occur mainly as disseminated grains or as inclusions in partially limonitized pyrite.

Gold occurs in quartz, mainly as electrum, as isolated anhedral grains (7 to 200 μm) and also as inclusions (<50 μm) in pyrite and associated with silver. Occasionally, electrum and pyrite are intergrown and develop simplectitic textures. Small dendritic grains and octahedral and dodecahedral crystals of gold (0.25 to 0.7 mm) were

identified in the walls of small cracks and cavities of quartz veins. In general gold fineness ranges between 838 and 522.

Silver is scarce, but slightly more abundant than higher-fineness gold, it occurs in quartz as anhedral grains associated with pyrite and electrum, developing intergrowths and aggregates, and also associated with stützite and cervelleite.

Acanthite occurs as small, anhedral grains (<50 μm), commonly associated with gold and uytenbogaardtite; the chemistry of these grains may show local enrichment in selenium.

Stromeyerite occurs as irregular aggregates, associated with pyrite and occasionally intergrown with chalcocite developing myrmekitic textures, following the stromeyerite cleavage (Ramdohr 1980, Bergstöl and Vokes 1974); the oleander leaf texture is locally developed. Digenite and covellite may replace stromeyerite. The chemical composition of this mineral is generally enriched in Cu at the expense of Ag.

Uytenbogaardtite was observed as anhedral grains, up to 37 μm , closely associated with gold and acanthite, occasionally with minor amounts of oxidized pyrite and chalcopyrite partially replaced by covellite (\pm limonite) and pyrrhotite. The results of the electron microprobe analyses (Mugas Lobos *et al.* 2011, 2012a) show Ag enrichment and S and Au depletion compared to its ideal chemical composition.

Naumannite occurs as very scarce individual grains of small size (50 μm in average) in quartz and frequently associated with gold.

Polybasite occurs in quartz as small irregular grains (~ 50 μm) associated with gold, silver and chalcopyrite, where polybasite selective and centripetally replaces the later. The chemical composition shows an enrichment in Se at the expense of S, but still low enough for the mineral to be polybasite (S:Se ~ 4.5:1).

Stützite and cervelleite are present as irregular grains up to 400 μm , either isolated, or related to silver and occasionally to pyrite. Cervelleite partially replaces stützite.

Supergenic minerals: Chalcocite, digenite and covellite are closely related to each other, commonly replacing chalcopyrite. Occasionally, chalcocite and stromeyerite

occur as intergrowths and digenite partially replaces the latter. In general, digenite replaces chalcopyrite, chalcocite and in a lesser degree bornite; covellite mainly replaces chalcopyrite, chalcocite and digenite.

Anglesite is very scarce and locally replaces galena in reduced areas.

Hematite usually partially to totally replaces pyrite and magnetite and is commonly found filling pyrite boxworks and cracks in quartz.

Goethite occurs as colloform and botryoidal aggregates, commonly replacing pyrite.

FLUID INCLUSION STUDIES

Petrography and microthermometry

The microthermometric studies were performed in petrographically defined FIAs, with populations of at least three fluid inclusions. All analyzed fluid inclusions were primary, small (<10 μm), mainly irregular, biphasic (liquid-vapor) and belonging to all stages of the mineralization but the stage 6, due to the lack of suitable FIAs. No carbonic phases were detected during microthermometric runs. In these low salinity fluid inclusions, the vapor bubbles occupy from 10 to 40% of the inclusion volume; in FIAs with boiling evidences these percentages are highly variable, from 10 to 95%. One hundred and nineteen melting temperatures and seventy-seven homogenization temperatures were obtained in quartz and fluorite samples (Table 1). The results indicate that fluid inclusions in quartz have average salinities in a range between 2.16 and 5.16 wt% $\text{NaCl}_{\text{equiv}}$ and homogenization temperatures in a range between 205.2 and 316.0°C. The maximum values for salinity and homogenization temperature, 5.16 wt% $\text{NaCl}_{\text{equiv}}$ and 316.0°C, respectively, belong to the fluid inclusions of the stage 4a with petrographic and mineralogical evidences of boiling, characterized by veins with bladed quartz and small adularia crystals.

The fluid inclusions in fluorite have lower values, with salinities ranging from 0.79 to 1.28 wt% $\text{NaCl}_{\text{equiv}}$ and homogenization temperatures from 161.9 to 184.9°C. On the basis of the microthermometric results,

the evolution of temperature and salinity in the system was plotted in the Fig. 7, showing a temperature increase at first (1) up to the stage 4a, where the salinity reaches the maximum values; right after that, the fluids become more diluted (2) and finally the temperature, together with the salinity decrease to the minimum (3) values in the system.

LA-ICP-MS

After the microthermometry studies, eleven FIAs from a selected population of thirty-four were analyzed by LA-ICP-MS. All assemblages were selected on the basis of individual fluid inclusion size (>4 μm); in

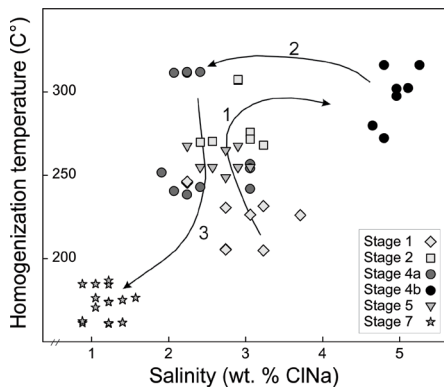


Figure 7. Homogenization temperature (°C) vs. salinity (wt% NaCl_{equiv.}) graphic. Arrows represent the tendency in fluid evolution. All microthermometric data from the different stages of mineralization were represented.

three occasions, where individual analyses were not feasible due to the small size of the inclusions, more than one inclusion in the assemblage were ablated together, giving an average set of values for the FIA. Microanalyses were performed in quartz from the stages of mineralization 2 to 5; accordingly, twenty-four fluid inclusions were ablated and the results are summarized in Table 2 and Figures 8 and 9; analytical limitation prevent the analyses of fluid inclusion hosted by fluorite. In general, low signals were common and many data were lost because quartz cracking was extensive during ablation. Fluid inclusions in general show measurable quantities of Na, K and Sb and variable quantities of S, Fe, Cu, As, Ag and Pb (Fig. 8). Four fluid inclusions were an-

TABLE 1. Microthermometric data of primary fluid inclusions in quartz and fluorite from Don Sixto mining project

Stages	Sample-FIA #	Salinity (wt% NaCl _{equiv.})					T _h (°C)				
		Max	Min	Avg.	SD	n	Max	Min	Avg.	SD	n
1 (Qz)	163-1	3.71	3.06	3.28	0.4	3	226.3	226.0	226.1	0.2	2
	163-2	3.87	3.55	3.71	0.2	3	---	---	---	---	-
	54-9	3.23	2.74	2.95	0.2	3	231.5	230.6	231.0	0.7	2
	54-10	3.23	2.74	2.90	0.3	3	205.6	204.8	205.2	0.4	3
	54-11	2.57	2.07	2.28	0.2	4	246.2	245.5	245.8	0.5	2
2 (Qz)	45-1	---	---	---	---	-	274.2	269.0	271.6	3.6	2
	45-5	2.90	2.74	2.85	0.1	3	307.6	307.1	307.3	0.4	2
	45-6	3.23	2.57	2.98	0.3	4	270.3	248.7	262.4	11.9	3
	45-2	3.06	2.57	2.90	0.3	3	275.8	271.7	273.7	2.9	2
	45-3	2.57	2.07	2.32	0.2	4	269.8	---	---	---	1
3 (Qz)	54-6	2.90	2.57	2.74	0.2	3	---	---	286.9	18.1	-
	54-7	2.74	2.24	2.41	0.3	3	---	---	---	---	-
	54-11	2.57	2.24	2.41	0.1	4	---	---	---	---	-
4a (Qz)	49-2	4.65	---	---	---	1	298.5	279.7	288.2	9.5	3
	49-3	5.26	4.65	4.90	0.3	3	316.0	316.0	316.0	0.0	2
	49-5	5.11	4.96	5.01	0.1	3	302.7	297.4	301.0	2.4	4
	49-1-10	5.41	4.80	5.11	0.3	3	---	---	---	---	0
	49-13	5.11	4.80	4.90	0.2	3	272.2	---	---	---	1
	49-14	4.96	4.80	4.88	0.1	2	---	---	---	---	-
	49-9	5.26	5.11	5.16	0.1	3	---	---	---	---	-
	49-2-10	---	---	---	---	-	275.6	273.6	274.7	1.1	4
	49-2-14	5.11	4.80	4.96	0.2	3	---	---	---	---	-
	4b (Qz)	111-1	3.06	2.74	2.95	0.2	3	256.5	---	---	---
111-3		3.06	2.57	2.82	0.2	4	---	---	---	---	-
111-6		3.06	2.74	2.90	0.1	4	---	---	---	---	-
111-8		2.41	1.91	2.16	0.2	4	269.0	238.2	248.4	12.6	5
111-9		3.06	3.06	3.06	0.0	3	254.0	241.7	247.9	8.7	2
154-2		2.57	2.07	2.36	0.2	4	---	---	---	---	-
154-1		2.57	2.41	2.52	0.1	3	---	---	---	---	-
154-7		---	---	---	---	-	312.0	311.9	311.9	0.0	5
154-9		2.41	2.07	2.24	0.1	4	311.9	311.4	311.6	0.3	4
59-1		2.90	2.24	2.63	0.3	3	267.6	265.0	266.7	1.5	3
5 (Qz)	59-2	3.06	2.74	2.90	0.2	3	254.8	248.7	252.8	3.5	3
	59-3	2.90	2.41	2.63	0.2	3	254.8	254.8	254.8	0.0	3
	155-6	1.57	1.05	1.27	0.3	4	176.4	170.5	174.4	3.3	3
7 (Fl)	155-9	1.40	1.22	1.28	0.1	3	175.0	173.8	174.5	0.7	4
	155-10	1.40	0.88	1.12	0.1	5	164.2	160.8	161.9	1.2	6
	155-11	0.88	0.70	0.79	0.1	4	---	---	---	---	---
	155-12	1.22	0.88	1.09	0.2	4	186.8	183.8	184.9	1.1	5
	155-12	1.22	0.88	1.09	0.2	4	186.8	183.8	184.9	1.1	5

The values in italics were calculated from average values from the stages 2 and 4a based on interpretations from Fig. 7. Qz: quartz, Fl: fluorite.

alyzed from the stage 1, but all elements were under the detection limits.

Along the different stages of mineralization Na quantities vary in between 7,193 and 17,596 ppm, with its lower values in the stage 2, and the highest values in the stage 4a. Potassium content has a similar pattern to that of Na, the highest values measured in the stage 5 (11,070 ppm); the dispersion diagram showing the relation between Na and K indicate a negative correlation between these elements (Fig. 9a). Sulfur was detected in only three isolated inclusions belonging to stages 4b and 5 (Table 2).

Iron and Cu were detected in almost every stage of mineralization (Figs. 8, 9b, Table 2) and their quantities vary significantly,

reaching their maximum amounts in the stage 4a.

Antimony was observed in most of the mineralizing stages from Don Sixto, in the inclusion fluids and in the host quartz; the content of this element is up to 13,095 ppm (Table 2, Fig. 9c). Silver and lead were identified in low quantities, with their higher amounts detected in the stage 2 and 5 in the former, and stages 4a and 5 in the latter (Table 2, Figs. 9d, e). The same was observed for arsenic, only detected in the stages 3 (107 ppm) and 4a (176 ppm).

Cesium contents are variable in a range between 3 and 207 ppm. In relation to sodium, Cs has a well-defined negative correlation for most of the stages (Fig. 9f).

Gold was detected in only one fluid inclu-

sion from the stage 4b, going up to 5 ppm. On the basis that the limit of detection was 1.70 ppm, the measured value is considered a true value.

STABLE ISOTOPES

The oxygen and sulfur isotopic fractionation was analyzed in seven quartz and two pyrite samples from Don Sixto deposit. The resulting $\delta^{18}\text{O}$ and $\delta^{34}\text{S}$ values in quartz and pyrite samples from the stages of mineralization 2, 3, 4, 5 and 6 (Table 3) were used to calculate the isotopic fractionation factor of quartz-H₂O and pyrite-H₂S, where the equations of Zheng (1993) and Ohmoto and Rye (1979) were

TABLE 2. Summary of LA-ICP-MS results (ppm) of primary fluid inclusion assemblages from Don Sixto

Stage	Sample-FIA #	Na	S	K	Fe	Cu	As	Ag	Sb	Cs	Au	Pb
2	45-5	7193	<72613	9477	<15244	<256	<660	<69	11257	60	<30	<51
2	45-5	9311	<36413	5565	17492	<92	<316	<36	5551	18	<11	<24
2	45-5	10995	<8844	1095	1879	<24	<77	<8	805	8	<3	<7
2	45-6	11274	<28021	3809	<6121	<98	<245	<28	917	13	<10	<19
2	45-6N	10823	<27359	1446	<6238	109	<261	28	1677	17	<11	<18
2	45-6N	9727	<37904	4445	<8590	<141	<357	<37	<54	16	<15	35
2	45-6N	11348	<54143	<2698	<11435	176	<502	<49	<70	21	<19	<32
3	54-7	8292	<5300	1367	2612	<20	107	15	1877	21	<1	<3
3	54-7	9317	<72605	<3617	<15785	335	<714	<73	1296	207	<29	<55
4a	49-8	17596	<2738	10720	31737	646	176	<137	<164	118	<5	104
4b	111-9	8011	<84127	10644	<20168	<327	<805	<98	8787	40	<40	<63
4b	111-9	10947	<97133	<4715	<22331	<360	<935	<106	<159	37	<42	<86
4b	111-9	11590	<12093	1178	<2766	<43	<115	<12	9112	9	<4	<10
4b	111-Z	10677	6765	<283	<1385	<22	<53	4	<8	3	<2	3
4b	111-Z	10362	<4458	1098	<1102	<18	<42	<3	<6	5	<1	3
4b	111-Z	9774	<4895	2655	<1172	25	<43	5	<6	5	5	<2
4b	111-6*	10934	<5198	1253	3049	<26	<48	<5	<7	5	<1	7
5	59-1	8387	<31450	6229	<4269	<116	<186	<38	<22	61	<12	124
5	59-1	9673	<10750	1115	<1459	42	<63	41	2047	14	<4	6
5	59-1	9436	<30118	1778	4274	<83	<175	<31	6363	27	<10	<6
5	59-1	7901	<45761	5757	<5877	<132	<259	<47	11417	157	<16	39
5	59-1	9674	72840	<1497	<7988	<181	<354	<64	13095	57	<22	<13
5	59-3*	9468	31659	1468	<1869	230	<83	663	<8	14	<4	64
5	59-2*	7215	<51672	11070	<6437	<153	<275	84	<32	22	<12	38

* = more than one inclusion ablated together. Limits of detection in italics.

used together with their average homogenization temperatures following Beaudoin and Therrien (1999-2016). The $\delta^{18}\text{O}_{\text{H}_2\text{O}}$ and $\delta^{34}\text{S}_{\text{H}_2\text{S}}$ calculations were done right after. Due to the lack of homogenization temperatures for every stage, the isotopic fractionation of the hydrothermal fluid was not calculated for all quartz and pyrite samples (Table 3).

The isotopic fractionation of oxygen in quartz samples from the stages 2, 3, 4 and 5 are in the range of 1.11 to 4.41 ‰, relative to VSMOW (Table 3). The calculated oxygen fractionation of the hydrothermal fluid, in equilibrium with the crystallizing quartz, was in the range between $\delta^{18}\text{O}_{\text{H}_2\text{O}} = -6.92$ and -3.29 ‰, which is coherent with a meteoric water source.

The obtained $\delta^{34}\text{S}$ values were 1.77 and 2.37 ‰, relative to VCDT, for the stages of mineralization 6 and 4a respectively. Considering the average homogenization temperature of the stage 4a (295°C), the calculated $\delta^{34}\text{S}_{\text{H}_2\text{S}}$ value was 1.17 ‰.

GEOCHRONOLOGY

In order to analyze the age of the alteration-mineralization process in Don Sixto deposit, adularia crystals from the stage 2 were selected and dated by the $^{40}\text{Ar}/^{39}\text{Ar}$ multiple step heat method. The resulting plateau age with ~80 % of the gas released was 252.7 ± 1.3 Ma, this result directly links the mineralization in Don Sixto with its gondwanic host rocks. Antecedents in Argentina indicate that epithermal mineralizations related to the gondwanic magmatism are scarce, only Cerro Casposo (San Juan) with a K/Ar age of 280 ± 9 Ma in adularia (Sotarello *et al.* 2004) has a certain gondwanic age.

DISCUSSION AND CONCLUSIONS

Don Sixto is a low sulfidation epithermal deposit (Hedenquist 1987), containing the low sulfidation pair, pyrite-arsenopyrite, within banded veins of quartz and adularia (\pm chalcedony) plus subordinated calcite (Sillitoe and Hedenquist 2003). The mineralization in this area is hosted in epithermal quartz veins and volcanic-pyroclastic

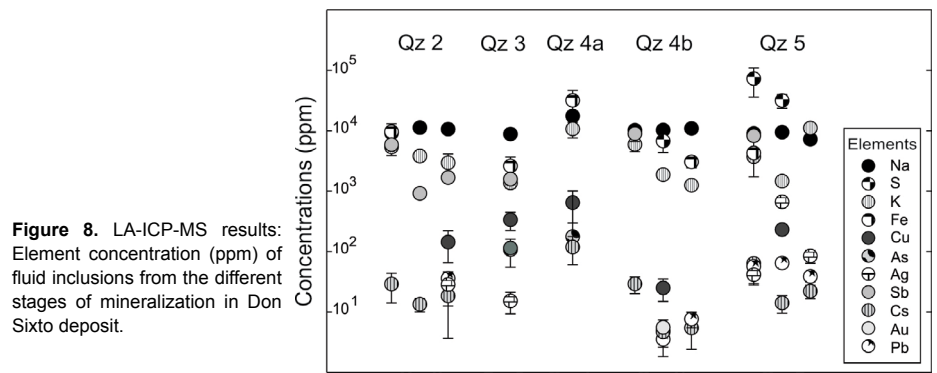


Figure 8. LA-ICP-MS results: Element concentration (ppm) of fluid inclusions from the different stages of mineralization in Don Sixto deposit.

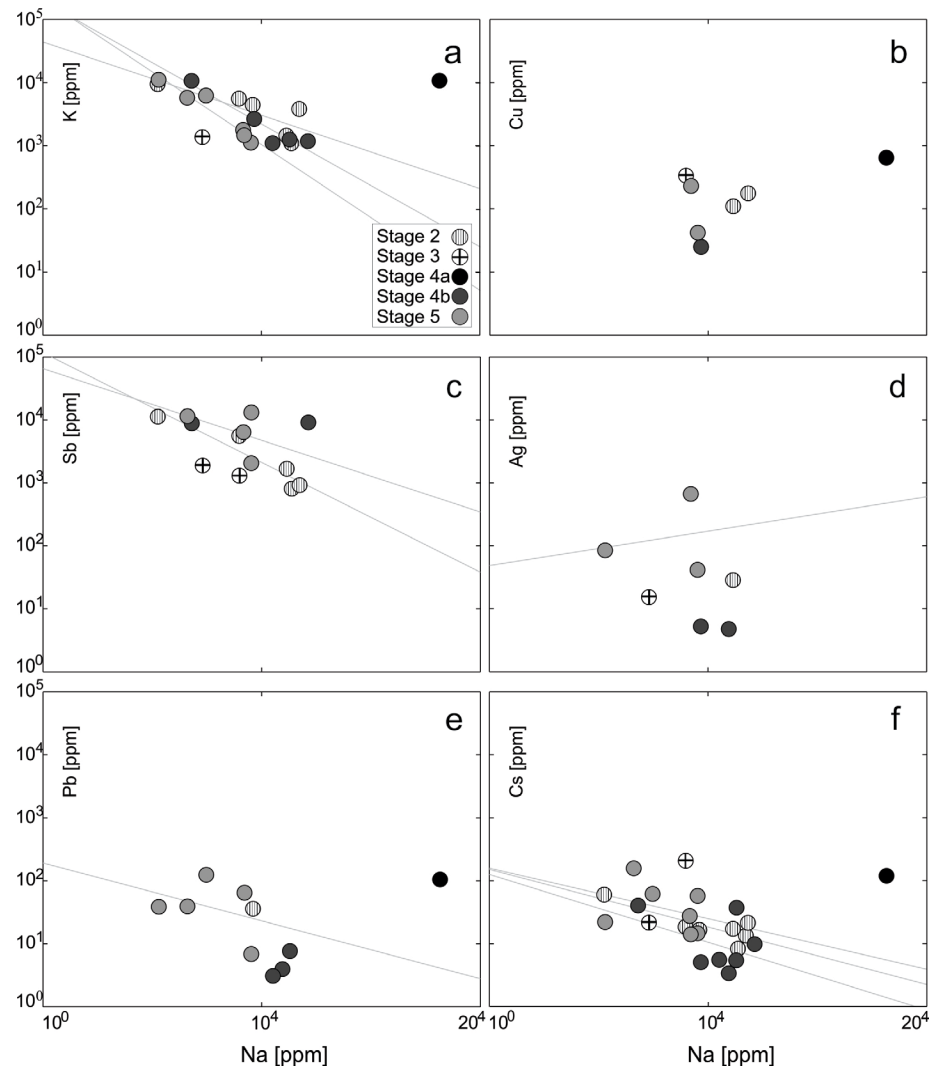


Figure 9. Dispersion diagrams using all LA-ICP-MS results: a) Na vs. K; b) Na vs. Cu; c) Na vs. Sb; d) Na vs. Ag; e) Na vs. Pb; f) Na vs. Cs; Regression lines were plotted whenever possible.

units of the Choique Mahuida Formation and El Portillo Group, local gondwanic rocks representative of the Choiyoi magmatism. With an age of 252.7 ± 1.3 Ma, Don Sixto is one of a few low sulfidation deposits of Permian-Triassic age in Argen-

tina related to the Choiyoi metallogeny. Reflectance spectroscopy data led to the recognition of illite group minerals: illite, smectite and lesser kaolinite \pm chlorite, goethite and hematite with buddingtonite in close relationship to illite and high av-

TABLE 3. Isotopic fractionation of oxygen and sulfur from vein samples

Stages	Sample #	Mineral	T _h °C	δ ¹⁸ O _{Qz}	δ ³⁴ S _{Py} (‰)	δ ¹⁸ O _{H2O} (‰)	δ ³⁴ S _{H2S} (‰)
2	45	Qz	279	3.63 ± 0.04	—	-4.17	—
3	159	Qz	287	1.82 ± 0.05	—	-5.68	—
	101	Qz	287	2.51 ± 0.05	—	-4.99	—
4a	49	Qz	295	1.11 ± 0.01	—	-6.09	—
	155	Py	295	—	2.37	—	1.17
4b	161	Qz	280	4.41 ± 0.05	—	-3.29	—
5	173	Qz	258	1.68 ± 0.02	—	-6.92	—
	143	Qz	258	3.74 ± 0.03	—	-4.86	—
6	15	Py	—	—	1.77	—	—

Th °C = average temperature; Qz= quartz; Py= pyrite.

erage Au grades (1.63 g/t, Ojo prospect). In exploration for gold mineralization buddingtonite is highly appreciated because it is considered a guide to gold, though scarce information has been published to confirm this observation. In the low sulfidation Banderas prospect in Guatemala, Harlap (2008) indicated that buddingtonite is abundant as a product of ammonium alteration and it is closely related to gold. Moreover, this author interpreted that considering the association of buddingtonite and gold it is possible to speculate that ammonia complexes may play an important role in gold transportation, being a very reliable vector to epithermal gold mineralization in some environments. Also, Krohn *et al.* (1993) indicated that the high ammonium content in the hydrothermal systems in western U.S., the close association to mercury and the small crystal size of the ammonium-bearing minerals in these systems, all suggest that ammonium may be transported in a late-stage vapor phase or as an organic volatile. The presence of highly crystalline illite and buddingtonite in Don Sixto deposit, together with gold mineralization is encouraging on the basis that it has been proposed that illite crystallinity and ammonium alteration intensity increases towards gold mineralization (Harlap 2008). To confirm these observations and test the buddingtonite-gold relationship, detailed studies are required. The study of Don Sixto epithermal vein

system led to the recognition of seven stages of mineralization where quartz is the major gangue mineral and is typically the only phase deposited throughout the life span of the hydrothermal system; adularia and fluorite (± calcite) are also present in minor quantities. The features of vein textures in every stage of mineralization indicate that primary growth textures are most abundant; massive, crustiform, comb and zoned textures may be the result of episodic pressure release for crustiform banding and slow changing conditions during crystal growth for comb and zoned textures (Dong *et al.* 1995). Bladed replacement textures with adularia crystals (± calcite), which are typical evidences of a boiling process, were recognized in the stages 2 and 4a. On the bases of fluid inclusion petrography the stage 2 has no evidence of boiling, whereas the stage 4a has coexisting liquid-rich and vapor-rich fluid inclusions that indicate fluid boiling (Bodnar *et al.* 1985). The presence of rhombic and pseudo-acicular adularia crystals indicate that boiling conditions were protracted (Dong and Morrison 1995); observations in concordance with adularia crystals in the hydrothermal veins from Don Sixto deposit. Base metal minerals are widespread; abundant pyrite with lesser arsenopyrite, chalcopyrite and sphalerite are commonly present in most of the quartz veins. The precious metal minerals together with

Se-enriched, selenide and telluride minerals, occur mainly in the stages 4a and 4b (Fig. 6). Ciobanu *et al.* (2006) indicate that tellurides (and selenides) of Au, Ag, Bi, Pb, and other elements are commonly reported as trace minerals associated with gold in metallogenic belts and regions of various ages, and in individual deposits that span the magmatic-hydrothermal spectrum; the presence of stützite and cervelleite, in close association with silver grains is coherent with these observations. Moreover, Ciobanu *et al.* (2006) indicate that repetitive boiling is believed to account for gold precipitation, with simultaneous separation of tellurium into the vapor phase; these vapors could migrate upwards and condensate during mixing with superficial waters, depositing Au-(Ag)-tellurides, which matches well with the characteristics of stage 4.

A complete fluid inclusion petrography and subsequent microthermometry was performed in Don Sixto, considering that fluid inclusions provide a means of studying the fluids that are related to magmatic-hydrothermal ore deposits and to examine the possible mechanisms leading to their formation (Audétat *et al.* 2008). In quartz samples, main results indicate that salinities and temperature increase progressively in the subsequent mineralizing stages up to the stage 4, where evidences of boiling were identified together with the main precious metal mineralization. Right after, the fluids become more diluted, decreasing their salinities and temperatures (Fig. 7, Table 1).

LA-ICP-MS results indicate that, in general, hydrothermal fluids were diluted and the highest values of Na were reached in the stage 4a (Table 2, Fig. 8). Sodium average values ranging from 7,193 to 17,596 ppm are similar to absolute values obtained in other adularia-sericite deposits reported by Simpson *et al.* (2015): Karangahake (~260-10,200 ppm) and Martha and Favona (~440-9,600 ppm in quartz; ~9,680-13,700 ppm in amethyst), in Southern Hauraki Goldfield (New Zealand). Dispersion diagrams with their corresponding regression line, whenever possible, were prepared to test the relation between Na and different elements. In general, most of them show undefined trends (Figs.9b-e), changing correlations

significantly for the different stages; this situation is coherent with a limited number of results (Table 2).

The speciation of base and associated metals such as Cu, Fe, Zn, Pb, Cd and Ag is largely dominated by chloride complexes (Kouzmanov and Pokrovski 2012); in Don Sixto deposit, the maximum salinity measured in the stage 4 is associated with the highest amounts of Cu (646 ppm), Fe (31,737 ppm) and a high value of Pb (104 ppm). Cline and Bodnar (1991) indicate that the latest fluids to exsolve, in shallow systems (<~ 1.3 kbar), transport most of the chlorine and copper from the melt; though this observation might be confirmed in Don Sixto where the highest Cu and Na contents were reached together in the stage 4 (Table 2), more data is required to get a better understanding of these elements complexation.

The correlation observed between Na and Sb (Fig. 9c) is undefined, changing from negative to positive while the different stages were progressing in time. In this regard, experimental studies have determined that Sb and As are not complexed with chloride in solution but are transported as the stable neutral hydroxyl complexes of $\text{Sb}(\text{OH})_3$ and $\text{As}(\text{OH})_3$ over a wide range of temperatures (Simpson *et al.* 2015 and references therein). In the study area Sb was detected in most inclusion fluids (805-13,095 ppm) and also in the host quartz (8,602 ppm, stage 2). Moreover, concentrations of antimony in the host quartz were obtained when measuring quartz concentrations for host and background corrections; variable quantities were observed in every stage: 2 (11-107 ppm), 3 (29-99 ppm), 4a (13-119 ppm), 4b (5-340 ppm) and 5 (59-295 ppm). In this regard, it is considered that the presence of this element may be related to Sb-bearing minerals like polybasite and boulangerite that did precipitate in the stages 3 and 4, or maybe due to micro- or nano-scale inclusions in the host quartz. Antimony is a common component in low-sulfidation epithermal deposits like Southern Hauraki Goldfield (Simpson *et al.* 2015), where this element is commonly incorporated into the host quartz and amethyst preventing a constrained calculation of absolute concentrations of Sb in many inclusions, which is also the case

for Don Sixto deposit. Antimony concentrations in Karangahake (16 to -2,167 ppm, Simpson *et al.* 2015) are similar to Don Sixto values, considering that antimony was detected in the fluid inclusions as much as in the host quartz.

According to Audétat *et al.* (2008), the fluids with highest mineralization potential (high metal content and significant Cs content goes up to 100 ppm. In Don Sixto deposit, Cs contents vary significantly in between 3 and 207 ppm, with the highest contents reached in the stages 4a (118 ppm), 5 (up to 157 ppm) and 3 (up to 207 ppm); in general these values match well with Cs contents of potentially high mineralizing fluids, indicating that even the fluids with the highest Cs contents should have been present in significant volumes in order to contribute to the mineralization, like the fluids in the W (Bi)-mineralized part of the Mole Granite containing >100 ppm Cs (Audétat *et al.* 2008).

Even though only one inclusion shows a real content in Au (stage 4b), it belongs to the same sample where the only real signal for S was measured, and it is in excess relative to Fe, as it was also measured by Márquez-Zavalía and Heinrich (2016) in Alto de la Blenda, Farallón Negro Volcanic Complex, Argentina and previously theoretically predicted from thermodynamic modeling (Rauchenstein-Martinek *et al.*, 2014 and references therein) for Au solubility in low-salinity aqueous fluids derived from magmatic vapor.

Heinrich *et al.* (2004) indicated that if the initial fluid contains an excess of H_2S over FeCl_2 , pyrite precipitation cannot consume the entire reduced S, which therefore remains available for gold complexation and effective precious-metal transport from porphyry to epithermal conditions; that seems to be the case for gold transportation in Don Sixto. The loss of gaseous constituents, such as H_2 and H_2S , accompanying boiling over the central parts of major up flows zones, is likely to be the major process inducing the deposition of minerals typical of the low- sulfidation type epithermal ore

deposits (White and Hedenquist 1990, Hedenquist and Lowenstern 1994).

The stable isotope studies in quartz vein samples indicate that the calculated $\delta^{18}\text{O}_{\text{H}_2\text{O}}$ = -6.92 to -3.29 ‰ is coherent with a meteoric water source and values obtained in epithermal systems elsewhere, e.g., -3.11 to -1.9 ‰ in Dorado-Monserat, Argentina (Echavarría 2004), -7 to +2 ‰ in Creede, USA (Taylor 1997) and -3 to -17 ‰ in Rico, USA (Larson 1987). Moreover, considering the observations of Truesdell *et al.* (1977), Scott and Watanabe (1998) and Faure *et al.* (2002), the oxygen enrichment observed in the $\delta^{18}\text{O}_{\text{H}_2\text{O}}$ values from -6.09 to -3.29 ‰, along the stage 4 may be ascribed to a boiling process. The results would also match the detailed observations of Hayashi *et al.* (2000, 2001) who demonstrated that the formation of epithermal veins is the result of intermittent opening of the system associated with boiling and allowing the interaction of mineralizing fluids with meteoric waters, leading to the precipitation of the precious metals. The possibility of a magmatic input, as suggested by some authors for both, active geothermal systems (e.g., Hedenquist and Aoki 1991, Seki 1991, Giggenbach 1992) and mineralized epithermal systems (e.g., O'Neil and Silberman 1974, Matsuisha and Aoki 1994) is probable on the basis of the previous observations; magmatic fluids are commonly present in hydrothermal systems but their signature may be masked or erased owing to late overprinting by large volumes of meteoric water, which represents >95 % of the water ultimately convected during cooling of an intrusion in the shallow crust (Hedenquist and Lowenstern 1994).

As an approximation, the only result obtained for sulfur fractionation $\delta^{34}\text{S}_{\text{H}_2\text{S}}$ = 1.17 ‰ does not define a unique source for sulfur, a mixed one is possible between magmatic (0 ± 2 ‰ Ohmoto and Rye 1979) and granitic rocks (-10 to + 15 ‰ Coleman 1977), probably the acidic volcanic rocks from the Choique Mahuida Formation, with a possible contribution from the sedimentary rocks of the Agua Escondida Formation. It is evident that more detailed studies would be necessary to determine with certainty the source of sulfur.

ACKNOWLEDGMENTS

The authors are grateful to the Consejo Nacional de Investigaciones Científicas y Técnicas (CONICET), Argentina, for the financial support through the fellowships (ACML) and the grants PIP112-20090100857 and PIP 112-20120100554 (MAG, MFMZ). The LA-ICP-MS analytical parts of this study were supported by the Swiss National Science Foundation grant 200020_135302 (CAH). Special thanks are given to C. Heinrich for his financial help, the access to the microthermometry and LA-ICP-MS laboratories (ETH-Zürich) and for his helpful comments and suggestions on a previous draft. Authors are also grateful to Ex Torre Gold Mines Limited and Yamana Gold Inc. for giving access to the deposit, contributing with information and financial support, to P. Černý for the access to the electron microprobe facilities (U of M, Winnipeg, Canada), to R. Lira for giving access to the Fluid-Inc stage (Museo Alfred Stelzner, Universidad Nacional de Córdoba, Argentina), to M. Ordoñez for her help obtaining and interpreting the reflectance spectroscopy data and to D. Maier for introducing MFMZ to the SILLS program. The authors are grateful for the thorough reviews of the manuscript by M. Franchini and an anonymous referee, and for the suggestions and corrections made by the Associate Editor M. Lopez de Luchi.

REFERENCES

- Audétat, A., Pettke, T., Heinrich, C.A., and Bodnar, R. 2008. The composition of magmatic-hydrothermal fluids in barren and mineralized intrusions. *Economic Geology* 103: 877-908.
- Barton, P.B., and Bethke, P.M. 1987. Chalcopyrite disease in sphalerite: pathology and epidemiology. *American Mineralogist* 72: 451-467.
- Beaudoin, G., and Therrien, P. 1999-2016. AlphaDelta: calculateur du fractionnement des isotopes stables (Stable Isotope Fractionation Calculator). Département de géologie et de génie géologique, Université Laval, Québec, Canada. Available from URL: http://www2.ggl.ulaval.ca/cgi-bin/alphadelta/alphadelta_4alpha.cgi
- Bergstöl, S., and Vokes, F.M. 1974. Stromeerite and McKinstryite from the Godejord Poly-metallic Sulphide Deposit, Central Norwegian Caledonides. *Mineralium Deposita* 9: 325-337.
- Bodnar, R.J. 1993. Revised equation and table for determining the freezing point depression of H₂O-NaCl solutions. *Geochimica and Cosmochimica Acta* 57: 683-684.
- Bodnar, R.J. 2003. Re-equilibration of fluid inclusions. In: Samson, J., Anderson, A., Marshall, D. (eds.), *Fluid inclusions: analysis and interpretation*. Mineralogical Association of Canada, 213-230, Ottawa.
- Bodnar, R.J., and Vityk, M.O. 1994. Interpretation of microthermometric data for H₂O-NaCl fluid inclusions. In: De Vivo, B. and Frezzotti, M. L. (eds.), *Fluid Inclusions in Minerals, Methods and Applications*, Virginia Tech, 117-130, Blacksburg.
- Bodnar, R.J., Reynolds, T.J., and Kuehn, C.A. 1985. Fluid inclusion systematics in epithermal systems. In: Berger, B.R. and Bethke, P.M. (eds.), *Reviews in Economic Geology, Geology and Geochemistry of Epithermal Systems*, Society of Economic Geologist, 73-97, Littleton.
- Carpio, F., Mallimacci, H., Rubinstein, N., Salvarredi, J., Sepúlveda, E., Centeno, R., Rosas M., and Vargas, D. 2001. Metalogenia del Bloque de San Rafael, Mendoza. *Servicio Geológico Minero Argentino, Serie Contribuciones Técnicas, Recursos Minerales* 20: 1-109, Buenos Aires.
- Ciobanu, C.L., Cook, N.J., and Spry, P.G. 2006. Preface-Special Issue: Telluride and selenide minerals in gold deposits-how and why? *Mineralogy and Petrology* 87: 163-169.
- Clayton, R.N., and Mayeda, T.K. 1963. The use of bromine pentafluoride in the extraction of oxygen from oxides and silicates for isotopic analysis. *Geochimica and Cosmochimica Acta* 27: 43-52.
- Cline, J.S., and Bodnar, R.J. 1991. Can Economic Porphyry copper mineralization be generated by a typical calc-alkaline melt? *Journal of Geophysical Research* 96: 8113-8126.
- Coleman, M.L. 1977. Sulfur isotope in petrology. *Journal of the Geological Society* 133: 593-608.
- Deino, A.L. 2001. User's manual for Mass Spec 5.02: Berkeley Geochronology Center Special Publication 1a, 119 p., Berkeley.
- Delendatti, G.L. 2005. La Cabeza: Un Depósito Epitermal Aurífero de Baja Sulfuración en el Bloque de San Rafael, Mendoza, Argentina. 8 Congreso Argentino de Geología Económica, Actas 1: 199-206, Buenos Aires.
- Delendatti, G.L., and Williams, M.T. 2007. Don Sixto Project, Solid Geology 1225m RL. Unpublished Internal Report, Exeter Resource Corporation, 1p., Mendoza.
- Dong, G., and Morrison, G.W. 1995. Adularia in epithermal veins, Queensland: morphology, structural state and origin. *Mineralium Deposita* 30: 11-19.
- Dong, G., Morrison, G.W., and Jaireth, S. 1995. Quartz textures in epithermal veins, Queensland-classification, origin, and implication. *Economic Geology* 90: 1841-1856.
- Echavarría, L.E. 2004. Los fluidos hidrotermales formadores de la mineralización epitermal el Dorado-Monserrat, Macizo del Desierto. *Revista de la Asociación Geológica Argentina* 59: 70-82.
- Faure, K., Matsuhisa, Y., Metsugi, H., Mizota, C., and Hayashi, S. 2002. The Hishikari Au-Ag Epithermal Deposit, Japan: Oxygen and Hydrogen Isotope Evidence in Determining the Source of Paleohydrothermal Fluids. *Economic Geology* 97: 481-498.
- Giggenbach, W.F. 1992. Isotopic shifts in waters from geothermal and volcanic systems along convergent plate boundaries and their origin. *Earth and Planetary Science Letters* 113: 495-510.
- Godeas, M., and Rubinstein, N. 2004. Budding-tonita en el depósito epitermal El Pantanito, Mendoza. 7 Congreso de Mineralogía y Metalogenia, Actas 1: 61-62, Susques.
- Goldstein, R.H., and Reynolds, T.J. 1994. Systematics of Fluid Inclusions in diagenetic minerals. *SEPM Short Course 31*, Society for Sedimentary Geology, 199p., Tulsa.
- González Díaz, E.F. 1972. Descripción Geológica de la Hoja 27d, San Rafael, provincia de Mendoza. *Servicio Nacional Minero Geológico*, 127p., Buenos Aires.
- González Díaz, E.F., and García, H.H. 1966. El hallazgo del Neopaleozoico plantífero en el área de Agua Escondida (SE de Mendoza NO de La Pampa). 3 Jornadas Geológicas Argentinas, Actas 1: 341-354, Comodoro Rivadavia.
- Guillong, M., Meier, D.L., Allan, M.M., Heinrich, C.A., and Yardley, B.W.D. 2008. SILLS: A MATLAB-based program for the reduction of laser ablation ICP-MS data of homogeneous materials and inclusions. In: Sylvester, P. (ed.) *Laser ablation ICP-MS in the Earth Sciences: current practices and outstanding issues*. Mineralogical Association of Canada, 328-333, Vancouver.
- Günther, D., Audétat, A., Frischknecht, R., and

- Heinrich, C.A. 1998. Quantitative analysis of major, minor and trace elements in fluid inclusions using laser ablation inductively coupled plasma mass spectrometry. *Journal of Analytical Atomic Spectrometry* 13: 263-270.
- Harlap, A. 2008. Alteration and ammonium enrichment vectors to low-sulfidation epithermal mineralization: Insights from the Banderas gold-silver prospect. M.Sc. thesis (AAT MR51279), McGill University, 144p., Montreal.
- Hayashi, K.I., Maruyama, T., and Satoh, H. 2000. Submillimeter scale variation of oxygen isotope of vein quartz at the Hishikari deposit, Japan. *Resource Geology* 50: 141-150.
- Hayashi, K.I., Maruyama, T., and Satoh, H. 2001. Precipitation of gold in a low-sulfidation epithermal gold deposit: Insights from a submillimeter-scale oxygen isotope analysis of vein quartz. *Economic Geology* 96: 211-216.
- Hedenquist, J.W. 1987. Mineralization associated with volcanic-related hydrothermal systems in the Circum-Pacific basin. Transactions of the 4th Circum-Pacific Energy and Mineral Resources Conference, Circum-Pacific Council for Energy and Mineral Resources: 513-524, Singapore.
- Hedenquist, J.W., and Aoki, M. 1991. Meteoric interaction with magmatic discharges in Japan and the significance for mineralization. *Geology* 19: 1041-1044.
- Hedenquist, J.W., and Lowenstern, J.B. 1994. The role of magmas in the formation of hydrothermal ore deposits. *Nature* 370: 519-527.
- Heinrich, C.A., Pettke, T., Halter, W.E., Aigner-Torres, M., Audetat, A., Günther, D., Hattendorf, B., Bleiner, D., Guillong, M., and Horn, I. 2003. Quantitative multi-element analysis of minerals, fluid and melt inclusions by laser-ablation inductively-coupled plasma mass-spectrometry. *Geochimica et Cosmochimica Acta* 67: 3473-3497.
- Heinrich, C.A., Driesner, T., Stefánsson, A., and Seward, T.M. 2004. Magmatic vapor contraction and the transport of gold from the porphyry environment to epithermal ore deposits. *Geology* 32: 761-764.
- Kay, S.M., Ramos, V.A., Mpodozis, C., and Srugog, P. 1989. Late Paleozoic to Jurassic silicic magmatism at the Gondwana margin: Analogy to the Middle Proterozoic in North America? *Geology* 17: 324-328.
- Kleiman, L.E. 1993. El volcanismo Permo-Triásico y Triásico del Bloque de San Rafael (provincia de Mendoza): su potencial uranífero. 12 Congreso Geológico Argentino y 2 Congreso de Exploración de Hidrocarburos, Actas 5: 284-293, Mendoza.
- Kleiman, L.E., and Japas, M.S. 2009. The Choiyoi volcanic province at 34°S-36°S (San Rafael, Mendoza, Argentina): Implications for the Late Paleozoic evolution of the southwestern margin of Gondwana. *Tectonophysics* 473: 283-299.
- Kouzmanov, K., and Pokrovski, G.B. 2012. Hydrothermal controls on metal distribution in porphyry Cu (-Mo-Au) Systems. In: Hedenquist, J.W., Harris, M., Camus, F. (eds.), *Geology and genesis of major copper deposits and districts of the world: a tribute to Richard H. Sillitoe*. Society of Economic Geologists, Inc: 573-618, Littleton.
- Krohn, M.D., Kendall, C., Evans, J.R., and Fries, T.L. 1993. Relations of ammonium minerals at several hydrothermal systems in the western U.S. *Journal of Volcanology and Geothermal Research* 50: 401-413.
- Larson, P.B. 1987. Stable isotope and fluid inclusion investigations of epithermal vein and porphyry molybdenum mineralization in the Rico mining district, Colorado. *Economic Geology* 82: 2141-2157.
- Linares, E., Llambías, E.J., and Latorre, C.O. 1978. *Geología y Geocronología de las rocas eruptivas de la provincia de La Pampa*, República Argentina. 7 Congreso Geológico Argentino, Actas 1: 795-808, Neuquén, Argentina.
- Llambías, E.J. 1999. El Magmatismo Gondwánico durante el Paleozoico superior-Triásico. In: Caminos, R. (ed.), *Geología Argentina*. Instituto de Geología y Recursos Minerales, Anales 29: 349-376, Buenos Aires.
- Llambías, E.J., Kleiman, L.E., and Salvarredi, J.A. 1993. El Magmatismo Gondwánico. En Ramos, V.A. (ed.) *Geología y Recursos Naturales de Mendoza*. 12 Congreso Geológico Argentino y 2 Congreso de Exploración de Hidrocarburos, Relatorio 1: 53-64, Mendoza.
- Llambías, E.J., Quenardelle, S., and Montenegro, T. 2003. The Choiyoi Group from central Argentina: a subalkaline transitional to alkaline association in the craton adjacent to the active margin of the Gondwana continent. *Journal of South American Earth Sciences* 16: 243-257.
- Longerich, H.P., Günther, D., and Jackson, S.E. 1996. Elemental fractionation in laser ablation inductively coupled plasma-mass spectrometry. *Fresenius Journal of Analytical Chemistry* 355: 538-542.
- Márquez-Zavalía, M.F., and Heinrich, C.A. 2016. Fluid evolution in a volcanic-hosted epithermal carbonate-base metal-gold vein system: Alto de la Blenda, Farallón Negro, Argentina. *Mineralium Deposita* 51: 873-902.
- Matsuisha, Y., and Aoki, M. 1994. Temperature and oxygen isotope variations during formation of the Hishikari epithermal gold-silver veins, southern Kyushu, Japan. *Economic Geology* 89: 1608-1613.
- Mugas Lobos, A.C. 2012. Estudios mineralógicos, geoquímicos y metalogénéticos en el proyecto minero Don Sixto (ex La Cabeza), Mendoza, Argentina. Tesis doctoral, Universidad Nacional de Córdoba (inédita), 289p., Córdoba.
- Mugas Lobos, A.C., and Márquez-Zavalía, M.F. 2013. Fluid inclusion and stable isotope studies at Don Sixto, a precious metal low sulfidation deposit in Mendoza province, Argentina. *Resource Geology* 63: 350-359.
- Mugas Lobos, A.C., Márquez-Zavalía, M.F., and Galliski, M.A. 2010. Petrografía y geoquímica de las rocas gondwánicas del proyecto minero Don Sixto, Mendoza. *Revista de la Asociación Geológica Argentina* 67: 392-402.
- Mugas Lobos, A.C., Márquez-Zavalía, M.F., and Galliski, M.A. 2011. Selenium and precious metal-bearing minerals at Don Sixto mining project, Mendoza, Argentina. In: Barra, F., Reich, M., Campos, E. and Tornos, F. (ed.), *Let's talk ore deposits*. Proceedings of the 11SGA Meeting I: 708-710, Antofagasta.
- Mugas Lobos, A.C., Márquez-Zavalía, M.F., and Galliski, M.A. 2012a. Minerales de mena del depósito epitermal de baja sulfuración Don Sixto, Mendoza. *Revista de la Asociación Geológica Argentina* 69: 3-12.
- Mugas Lobos, A.C., Ordoñez, M., Márquez-Zavalía, M.F., and Galliski, M.A. 2012b. Spectral identification of buddingtonite and associated minerals at Don Sixto, a low sulfidation Au-Ag deposit. In: Hedenquist, J. and Fontboté, L. (comp.); Brandt, C. (ed.), *SEG Conference 2012, Integrated Exploration and Ore Deposits*: 1-3, Lima.
- Narciso, V., Zanettini, J.C., Santamaría, G., and Mallimacci, H.S. 2007. Hoja geológica 3769-II, Agua Escondida, provincias de Mendoza y La Pampa. Instituto de Geología y Recursos Minerales, SEGEMAR. 2 ed., Boletín 300, 54p., Buenos Aires.

- Ohmoto, H., and Rye, R.O. 1979. Isotope of sulfur and carbon. In Barnes, H.L. (ed.) *Geochemistry of Hydrothermal Deposits* 2nd ed. John Wiley & Sons: 509-567, New York.
- O'Neil, J.R., and Silberman, M.L. 1974. Stable isotope relations in epithermal Au-Ag deposits, *Economic Geology* 69: 902-909.
- Pettke, T., Halter, W.E., Webster, J.D., Aigner-Torres, M., and Heinrich, C.A. 2004. Accurate quantification of melt inclusion chemistry by LA-ICPMS: a comparison with EMP and SIMS and advantages and possible limitations of these methods. *Lithos* 78: 333-361.
- Ramdohr, P. 1980. *The ore minerals and their intergrowths* (2^o ed). Pergamon press, p 481-484.
- Ramos, V.A. 1999. Ciclos orogénicos y evolución tectónica. In: Zappettini, E.O. (ed.), *Recursos Minerales de la República Argentina*, SEGEMAR, Anales 35, 29-49, Buenos Aires.
- Rauchenstein-Martinek, K., Wagner, T., Wälle, M., and Heinrich, C.A. 2014. Gold concentration in metamorphic fluids: A LA-ICPMS study of fluid inclusions from the Alpine orogenic belt. *Chemical Geology* 385: 70-83.
- Renne, P.R., Swisher, C.C., Deino, A.L., Karner, D.B., Owens, T., and DePaolo, D.J. 1998. Intercalibration of Standards, absolute ages and uncertainties in ⁴⁰Ar/³⁹Ar dating, *Chemical Geology* 145: 117-152.
- Rocha-Campos, A.C., Basei, M.A.S., Nutman, A.P., and dos Santos, P.R. 2006. SHRIMP U-Pb zircon geochronological calibration of the Late Paleozoic Supersequence, Paraná Basin, Brazil. 5 South American Symposium on Isotope Geology: 322-325, Punta del Este.
- Rocha-Campos, A.C., Basei, M.A., Nutman, A.P., Kleiman, L.E., Varela, R., Llambias, E., Canile, F.M., and da Rosa O. de C.R. 2011. 30 million years of Permian volcanism recorded in the Choiyoi igneous province (W Argentina) and their source for younger ash fall deposits in the Paraná Basin: SHRIMP U-Pb zircon geochronology evidence. *Gondwana Research* 19: 509-523.
- Rubinstein, N., and Gargiulo, M.F. 2005. Análisis textural de cuarzo hidrotermal del depósito El Pantanito, provincia de Mendoza: Nuevos aportes sobre su génesis. *Revista de la Asociación Geológica Argentina* 60: 96-103.
- Rubinstein, N., Carpio, F., and Mallimacci, H. 2001. El depósito epitermal El Pantanito, provincia de Mendoza. *Revista del Instituto de Geología y Minería, UNJU* 14: 59-61.
- Scott, A.M., and Watanabe, Y. 1998. "Extreme boiling" model for variable salinity of the Hokko low-sulfidation epithermal Au prospect, southwestern Hokkaido, Japan. *Mineralium Deposita* 33: 568-578.
- Seki, Y. 1991. The physical and chemical structure of the Kukaizu geothermal system, Japan. *Geochemical Journal* 25: 245-265.
- Sillitoe, R.H., and Hedenquist, J.W. 2003. Linkages between volcanotectonic settings, ore-fluid composition, and epithermal precious metal deposits. In: Simmons, S.F., Graham, I. (eds.), *Volcanic, geothermal and ore-forming fluids: rulers and witnesses of processes within the earth*. Society of Economic Geologists, Inc: 315-343, Littleton.
- Simpson, M.P., Palinkas, S.S., Mauk, J.L., and Bodnar, R.J. 2015. Fluid inclusion chemistry of Adularia-Sericite epithermal Au-Ag deposits of the southern Hauraki Goldfield, New Zealand. *Economic Geology* 110: 763-786.
- Sotarello, G., Belvideri, I., Machuca, E., and Castro de Machuca, B. 2004. Cerro Casposo, Sistema Epitermal de Baja Sulfuración en el Área de Villa Corral, Calingasta, provincia de San Juan, Argentina. *Guía de Campo, Curso Latinoamericano de Metalogenia UNESCO, SEG 2004, Mendoza, Argentina*: 41-61.
- Steiger, R.H., and Jäeger, E. 1977. Subcommission on geochronology: Convention on the use of decay constants in geo- and cosmo-chronology. *Earth Planetary Science Letters* 36: 359-363.
- Stipanovic, P.N., Rodrigo, F.O.L., and Martínez, C.G. 1968. Las Formaciones preneonianas en el denominado Macizo Nordpatagónico y regiones adyacentes. *Revista de la Asociación Geológica Argentina* 23: 67-98.
- Taylor, H.P. Jr. 1997. Oxygen and hydrogen isotope relationships in hydrothermal mineral deposits. In: Barnes, H.L. (ed.), *Geochemistry of Hydrothermal Ore Deposits*. 3rd ed. John Wiley & Sons: 229-302, New York.
- Truesdell, A.H., Nathenson, M., and Rye, R.O. 1977. The effects of subsurface boiling and dilution on the isotopic compositions of Yellowstone thermal waters. *Journal of Geophysical Research* 82: 3694-3704.
- Van der Heyden, A., and Yeo, W. 2007. Technical Report: 2007 Revised resource estimation, Don Sixto Gold Project, Mendoza province, Argentina. Prepared for Exeter Resource Corporation, 640 p., Vancouver.
- White, N.C., and Hedenquist, J.W. 1990. Epithermal environments and styles of mineralization: variations and their causes, and guidelines for exploration. *Journal of Geochemical Exploration* 36: 445-474.
- Zheng, Y.F. 1993. Calculation of oxygen isotope fractionation in anhydrous silicate minerals. *Geochimica and Cosmochimica Acta* 57: 1079-1091.

Recibido: 13 de julio, 2017

Aceptado: 5 de abril, 2018